Cell Stem Cell
Article

Regulation of Glycolysis by Pdk Functions as a Metabolic Checkpoint for Cell Cycle Quiescence in Hematopoietic Stem Cells

Keiyo Takubo,[1,*] Go Nagamatsu,[1] Chiharu I. Kobayashi,[1] Ayako Nakamura-Ishizu,[1] Hiroshi Kobayashi,[1] Eiji Ikeda,[3] Nobuhito Goda,[4,5] Yasmeen Rahimi,[9] Randall S. Johnson,[6] Tomoyoshi Soga,[5,7] Atsushi Hirao,[5,8] Makoto Suematsu,[2] and Toshio Suda[1,*]

[1]Department of Cell Differentiation, The Sakaguchi Laboratory of Developmental Biology, Keio University School of Medicine, 35 Shinano-machi, Shinjuku-ku, Tokyo 160-8582, Japan
[2]Department of Biochemistry, Keio University School of Medicine and Japan Science Technology Agency (JST), Exploratory Research for Advanced Technology (ERATO), Suematsu Gas Biology Project, 35 Shinano-machi, Shinjuku-ku, Tokyo 160-8582, Japan
[3]Department of Pathology, Yamaguchi University Graduate School of Medicine, 1-1-1 Minami-Kogushi, Ube, Yamaguchi 755-8505, Japan
[4]Department of Life Science and Medical Bio-Science, School of Advanced Science and Engineering, Waseda University, 2-2 Wakamatsu-cho, Shinjuku-ku, Tokyo 162-8480, Japan
[5]Core Research for Evolutional Science and Technology, Japan Science and Technology Agency, Chiyoda-ku, Tokyo 102-0075, Japan
[6]Department of Physiology, Development & Neuroscience, University of Cambridge, Downing Street, Cambridge CB2 3EG, UK
[7]Institute for Advanced Biosciences, Keio University, 246-2, Mizukami, Kakuganji, Tsuruoka City, Yamagata 997-0052, Japan
[8]Division of Molecular Genetics, Cancer Research Institute, Kanazawa University, Kakuma-machi, Kanazawa 920-1192, Japan
[9]Department of Biochemistry and Molecular Biology, Indiana University School of Medicine, Richard L. Roudebush VA Medical Center, 1481 W. 10th Street, Indianapolis, IN 46202-2803, USA
*Correspondence: keiyot@gmail.com (K.T.), sudato@z3.keio.jp (T.S.)
http://dx.doi.org/10.1016/j.stem.2012.10.011

SUMMARY

Defining the metabolic programs that underlie stem cell maintenance will be essential for developing strategies to manipulate stem cell capacity. Mammalian hematopoietic stem cells (HSCs) maintain cell cycle quiescence in a hypoxic microenvironment. It has been proposed that HSCs exhibit a distinct metabolic phenotype under these conditions. Here we directly investigated this idea using metabolomic analysis and found that HSCs generate adenosine-5′-triphosphate by anaerobic glycolysis through a pyruvate dehydrogenase kinase (Pdk)-dependent mechanism. Elevated Pdk expression leads to active suppression of the influx of glycolytic metabolites into mitochondria. Pdk overexpression in glycolysis-defective HSCs restored glycolysis, cell cycle quiescence, and stem cell capacity, while loss of both Pdk2 and Pdk4 attenuated HSC quiescence, glycolysis, and transplantation capacity. Moreover, treatment of HSCs with a Pdk mimetic promoted their survival and transplantation capacity. Thus, glycolytic metabolic status governed by Pdk acts as a cell cycle checkpoint that modulates HSC quiescence and function.

INTRODUCTION

Stem cells are tissue-sustaining cells that generate differentiated progeny and are resistant to external stresses (Zon, 2008; Seita and Weissman, 2010). Although stem cells probably exhibit metabolic characteristics allowing them to meet diverse energy demands, it is not known whether their metabolic phenotype differs from that of transiently amplifying progenitors and terminally differentiated cells and, if so, how metabolic phenotypes directly define stem cell identity (Suda et al., 2011). Cells generate adenosine-5′-triphosphate (ATP), the major currency for energy-consuming reactions, through central carbon metabolism, including glycolysis and mitochondrial oxidative phosphorylation (OXPHOS). The mammalian HSC system is maintained by self-renewal of quiescent long-term (LT)-HSCs and subsequent generation of short-term (ST)-HSCs, multipotent progenitors (MPPs), and various lineage-restricted progenies (Zon, 2008; Seita and Weissman, 2010). Adult LT-HSCs are maintained in a hypoxic state in the bone marrow (BM) niche (Parmar et al., 2007; Takubo et al., 2010). LT-HSCs maintain cell cycle quiescence through precise regulation of levels of hypoxia-inducible factor-1α (HIF-1α), a transcription factor responsive to cellular and systemic hypoxia (Takubo et al., 2010).

LT-HSCs, which exhibit fewer mitochondria than progenitors (Kim et al., 1998; Simsek et al., 2010; Norddahl et al., 2011), are hypothesized to utilize anaerobic metabolism in the hypoxic endosteal zone. Although the ratio of ATP generation to glucose consumption under anaerobic glycolysis is inefficient compared with that supported by OXPHOS, the rate of ATP production under hypoxia potentially increases 100-fold compared to that supported by mitochondrial energy production under normoxia (Voet and Voet, 2010). HSCs are particularly sensitive to oxidative stress and show low endogenous ROS levels. Aberrant ROS generation could abrogate various stem cell properties including cell cycle quiescence, self-renewal, survival, and multilineage differentiation capacity in HSCs (Miyamoto et al., 2007; Kobayashi and Suda, 2012). Because various mutant mice defective in LT-HSC maintenance display a wide range of bioenergetic defects in vivo, achieving a stable metabolic state in

LT-HSCs is probably important for their maintenance (Liu et al., 2009; Nakada et al., 2010; Gurumurthy et al., 2010; Gan et al., 2010; Sahin et al., 2011). Recently, Simsek et al. reported that LT-HSCs show higher glycolytic capacity than do cells in whole BM, which consists primarily of lineage marker$^+$-differentiated cells (Lin$^+$ cells) (Simsek et al., 2010). This activity is regulated by Cripto-GRP78 signaling activated by HIF-1α (Miharada et al., 2011). However, it remains unclear whether these metabolic characteristics are common in primitive hematopoietic cells such as LT-HSCs and progenitors and required for their maintenance.

In this study, we addressed the proposed "metabolic stemness" of HSCs, namely glycolytic activation, using metabolomics and genetics. During glycolysis, glucose is converted to pyruvate and then anaerobically to lactate or aerobically to acetyl-CoA for use in mitochondrial metabolism. The conversion of pyruvate to acetyl-CoA is catalyzed by pyruvate dehydrogenase (PDH), whose activity is suppressed by phosphorylation by PDH kinases (Pdks) (Harris et al., 2002). We observed that LT-HSCs show HIF-1α-mediated Pdk activation, resulting in maintenance of glycolytic flow and suppression of the influx of glycolytic metabolites into mitochondria. Also, a glycolytic metabolic state was shown to promote LT-HSC cell cycle quiescence, an activity that could potentially be exploited to regulate the cell cycle in those cells in vitro and in vivo. In mice, loss of Pdk2 and Pdk4 resulted in defective maintenance of cell cycle quiescence and transplantation capacity and altered glycolytic metabolic properties in LT-HSCs. Treatment of LT-HSCs with a competitive inhibitor of PDH promoted maintenance of transplantation capacity in vitro. These observations suggest that Pdk-mediated antagonism of mitochondrial metabolism comprises a checkpoint required to establish a metabolic state favoring cell cycle quiescence of LT-HSCs.

RESULTS

Metabolomic Profiling of Central Carbon Metabolism in LT-HSCs and Their Progeny

To define specific metabolic characteristics of hypoxic LT-HSCs, we performed metabolome analyses with capillary electrophoresis time-of-flight mass spectrometry (CE-TOFMS) (Soga et al., 2003, 2006; Shintani et al., 2009) using at least 1×10^6 murine BM LT-HSCs (CD34$^-$Flt3$^-$ Lineage marker$^-$ Sca-1$^+$ c-Kit$^+$; CD34$^-$Flt3$^-$ LSK cells) and their progeny, including ST-HSCs (CD34$^+$Flt3$^-$ LSK cells), MPPs (CD34$^+$Flt3$^+$ LSK cells), myeloid progenitors (MPs; Lin$^-$ c-Kit$^+$ Sca-1$^-$ cells), and differentiated hematopoietic cells (Gr-1/Mac-1+ myeloid cells, CD4/CD8+ T cells, and B220+ B cells) to assess levels of intracellular metabolites functioning in central carbon metabolism. We replicated the analysis and show one representative result in Figure 1A and Figure S1A available online (Figure 1A is an extract of Figure S1A). Notably, fructose 1,6-bisphosphate (F1,6BP), a product of the rate-limiting step of glycolysis catalyzed by phosphofructokinase-1 (Pfk-1), was observed only in LT-HSCs and ST-HSCs (Figures 1A and S1A). Because F1,6BP is a strong allosteric activator of pyruvate kinase (PK) (Voet and Voet, 2010), LT-HSCs probably support glycolytic metabolism required to produce PK-dependent ATP. Because low levels of the Pfk-1 substrate fructose-6-phosphate were also observed in LT-HSCs, the rate-limiting Pfk-1 reaction is probably activated in LT-HSCs (Figures 1A and S1A). In addition, pyruvate, a by-product of PK-dependent ATP generation, accumulated to high levels in LT-HSCs (Figures 1A and S1A), while levels of phosphoenolpyruvate, a PK substrate, remained low (Figures 1A and S1A). Mitochondrial OXPHOS is fueled by the tricarboxylic acid (TCA) cycle. Among TCA cycle-related metabolites, 2-oxoglutarate (2-OG) and both acetyl-CoA and succinyl-CoA were not detected in any hematopoietic fraction (Figure S1A). In support of metabolomics profiling data shown in Figures 1A and S1A, we found that various glycolytic enzymes were more highly expressed in LT-HSCs than in progenitors or terminally differentiated cells (Figure S1B), suggesting that LT-HSCs utilize glycolysis for energy generation (Voet and Voet, 2010).

Interestingly, LT-HSC ATP levels were lowest among various primitive hematopoietic cell fractions in the BM (Figure 1B). The Side Population (SP) phenotype of LT-HSCs is marked by expression of the ATP-dependent transporter Bcrp1 (Goodell et al., 1996, 1997; Zhou et al., 2001) and maintained by intracellular ATP production. The SP phenotype of normal LT-HSCs was sensitive to treatment with the glycolytic inhibitor 2-deoxy-D-glucose (2-DG) (Figure 1C). Treatment of BM mononuclear cells (MNCs) with the respiration inhibitor sodium azide (NaN_3), even at concentrations (20 mM) sufficient to inhibit OXPHOS, moderately reduced SP phenotypes in LT-HSCs (Figure 1C). Glucose uptake by cells from primitive fractions including LT- or ST-HSCs or MPPs was higher than that seen in myeloid progenitor or lineage marker+ fractions (Figure 1D). The activity of pyruvate kinase, which catalyzes an ATP-generating step in glycolysis, was highest in LT-HSCs among various BM fractions (Figure 1E). Overall, these observations suggest that only LT-HSCs, rather than transiently amplifying progenitors or terminally differentiated cells, can survive independent of mitochondrial energy generation, possibly through suppression of the PDH-E1α subunit by Pdk-dependent phosphorylation (depicted schematically in Figure 2A). Expression of all murine Pdk family members (Pdk1–Pdk4) (Harris et al., 2002) was high in LT-HSCs (Figure 2B), and PDH-E1α was more highly phosphorylated in LT-HSCs than in their differentiated progeny (Figures 2C and 2D). The oxygen consumption rate (OCR) was lowest in LT-HSCs, dynamically upregulated after their differentiation into ST-HSCs, and slightly decreased in MPPs or MPs (Figure 2E). The higher OCR seen in fractions other than LT-HSCs was probably maintained by mitochondrial oxygen consumption, as treatment with oligomycin, which inhibits mitochondrial ATP synthase, clearly suppressed the OCR in these cells (Figure 2E). These findings are in accord with the idea that LT-HSCs survive in a hypoxic environment and are less dependent on mitochondrial oxygen-consuming metabolism than more differentiated cells (Figure 2E).

Loss of HIF-1α Alters Energy Metabolism in LT-HSCs

To determine whether a HIF-1α-dependent crucial checkpoint maintains anaerobic metabolic stemness in LT-HSCs, we examined parameters relevant to metabolism in *HIF-1*$\alpha^{\Delta/\Delta}$ LT-HSCs. We found that HIF-1α deficiency was accompanied by decreased expression of various glycolytic enzymes in LT-HSCs (Figure S2). Glucose uptake was identical at various differentiation stages in *HIF-1*$\alpha^{\Delta/\Delta}$ BM (Figure 3A), although an essential glucose transporter, Glut1, was significantly downregulated in

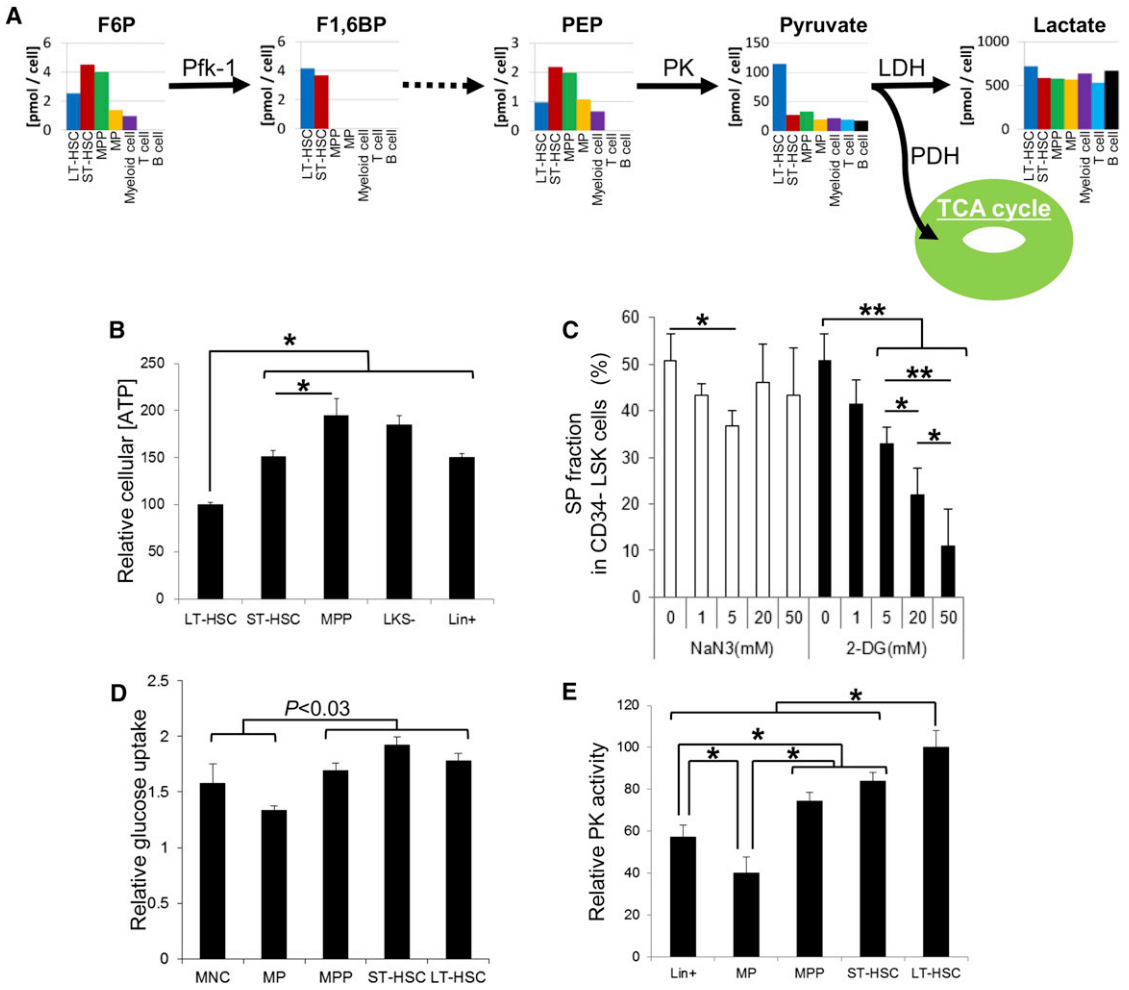

Figure 1. Metabolic Profiling of Glycolytic Metabolism in HSCs and Their Progeny

(A) Quantification of metabolites in glycolytic metabolism based on CE-TOFMS analysis. Bar graphs for independent metabolites plotted in the glycolytic metabolism map are (from left to right): long-term (LT)-hematopoietic stem cells (HSCs) ($CD34^-Flt3^-$ LSK cells; blue bars), short-term (ST)-HSCs ($CD34^+Flt3^-$ LSK cells; red bars), multipotent progenitors (MPPs) ($CD34^+Flt3^+$ LSK cells; green bars), myeloid progenitors (MPs; Lin^- c-Kit^+ $Sca\text{-}1^-$ cells; yellow bars), Gr-1/Mac-1^+ myeloid cells (purple bars), CD4/$CD8^+$ T cells (sky blue bars), and $B220^+$ B lymphocytes (black bars). Data are representative of two independent experiments.

(B) Relative intracellular ATP concentrations in LT-HSC, ST-HSC, MPP, LKS^-, and Lin^+ cells (mean ± SD, n = 6, *p < 0.001).

(C) Effects of NaN_3 (open bars) or 2-DG (closed bars) treatment on the Side Population phenotype of the $CD34^-$ LSK fraction at indicated concentrations (mean ± SD, n = 4, *p < 0.05, **p < 0.0002).

(D) Relative glucose uptake by LT-HSC, ST-HSC, MPP, MP, and Lin^+ cells (mean ± SD, n = 5).

(E) Relative PK activity in LT-HSC, ST-HSC, MPP, MP, and Lin^+ cells (mean ± SD, n = 6, *p < 0.001).

See also Figure S1.

HIF-1α$^{\Delta/\Delta}$ LT-HSCs (Figure S2). Glycolytic LDH activity in normal LT-HSCs was higher than that seen in $CD34^+$ LSK progenitors (the sum of ST-HSCs plus MPPs) and was decreased in *HIF-1α*$^{\Delta/\Delta}$ LT-HSCs (Figure 3B). We found that LT-HSCs release lactate into the culture medium only under hypoxia and those levels decrease in the case of HIF-1α deficiency (Figure 3C). Because intracellular levels of lactate, a product of the LDH reaction, in LT-HSCs and their differentiated progeny were unchanged (Figures 1A and S1A), we conclude that LT-HSCs probably rapidly release lactate generated by glycolysis into the extracellular space. Intracellular pyruvate levels, which are high in LT-HSCs (Figures 1A and S1A), were decreased by HIF-1α deficiency (Figure 3D). These data suggest that, in the hypoxic niche, LT-HSCs suppress flux of glycolytic metabolites into mitochondria for the TCA cycle and *HIF-1α*$^{\Delta/\Delta}$ LT-HSCs show defective conversion of pyruvate to lactate, an activity maintained through the suppression of PDH by Pdk. In support of this, phosphorylation of the α subunit of PDH-E1 is attenuated in *HIF-1α*$^{\Delta/\Delta}$ LT-HSCs (Figure 3E). Overall ATP production was considerably decreased in *HIF-1α*$^{\Delta/\Delta}$ LT-HSCs compared to *HIF-1α*$^{\Delta/\Delta}$ $CD34^+$ LSK progenitors (Figure 3F), suggesting that ATP production in the former is dependent on HIF-1α-dependent glycolysis and that mitochondrial metabolism is suppressed by Pdk. Overall mitochondrial mass in wild-type LT-HSCs was

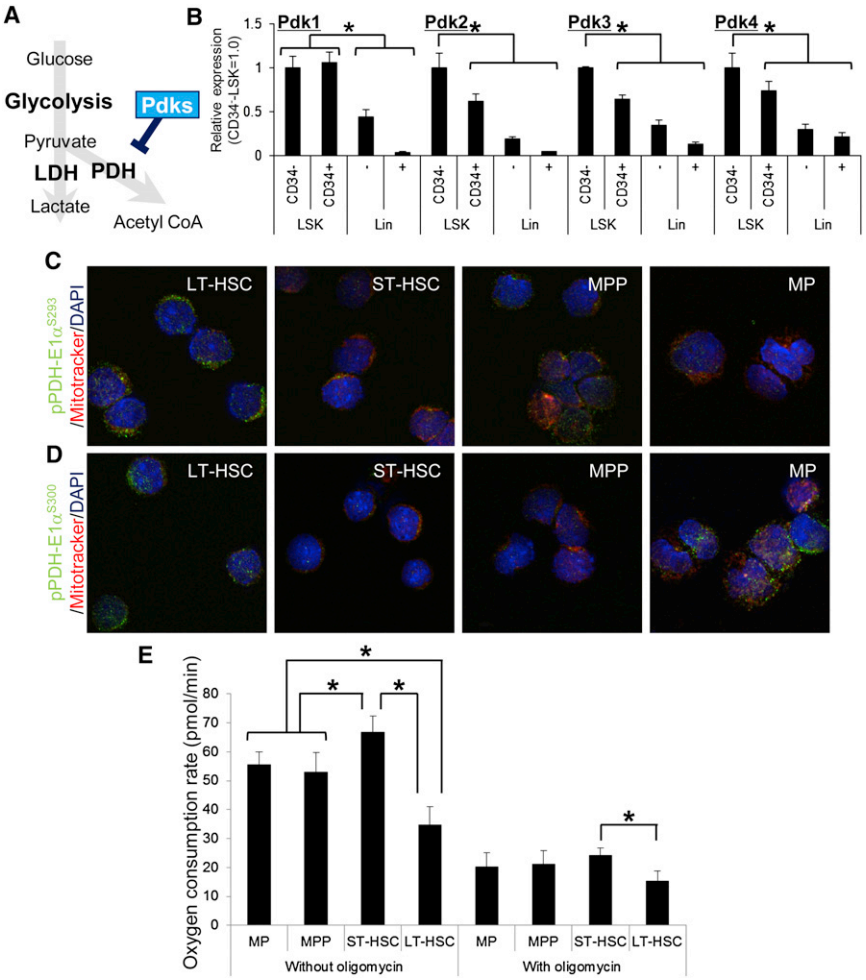

Figure 2. Pdk-Mediated Metabolic Properties of LT-HSCs

(A) Schematic representation of the effect of Pdks on energy metabolism.

(B) qPCR analysis of Pdk family members in $CD34^-$ LSK, $CD34^+$ LSK, Lin^-, or Lin^+ fractions from 12-week-old mice (mean ± SD, n = 4). Each value was normalized to β-actin expression and is expressed as fold induction compared to levels detected in $CD34^-$ LSK samples (*$p < 0.01$).

(C and D) Immunocytochemical staining for phosphorylated S293 (C) or S300 (D) residues of PDH-E1α (green), Mitotracker DeepRed (red), and DAPI (blue) in wild-type LT-HSC ($CD34^-$ $Flt3^-$ LSK), ST-HSC ($CD34^+$ $Flt3^-$ LSK), MPP ($CD34^+$ $Flt3^+$ LSK), or MP (Lineage marker$^-$ c-Kit^+ $Sca\text{-}1^-$) cells.

(E) Oxygen consumption rate in LT-HSC, ST-HSC, MPP, and MP cells treated with or without oligomycin (mean ± SD, n = 6) (*$p < 0.001$).

See also Figure S2.

smaller than that seen in wild-type $CD34^+$ LSK progenitors (Figure 3G). In *HIF-1α*$^{\Delta/\Delta}$ LT-HSCs, mitochondrial volume and expression of the mitochondrial respiratory component COX4-1 (Fukuda et al., 2007) were higher than that seen in wild-type LT-HSCs (Figures 3G and 3H). These data suggest that *HIF-1α*$^{\Delta/\Delta}$ LT-HSCs exhibit decreased dependence on anaerobic glycolysis and activate mitochondrial aerobic metabolism due to loss of a metabolic checkpoint regulated by PDH-E1α subunit phosphorylation status.

To directly analyze metabolic changes in *HIF-1α*$^{\Delta/\Delta}$ HSCs, we analyzed the SP phenotype. Overall, the *HIF-1α*$^{\Delta/\Delta}$ LSK fraction showed significant loss of the SP phenotype after treatment with 20 mM NaN_3 (Figure S3A), suggesting that, in the case of HIF-1α deficiency, compensatory mitochondrial aerobic metabolism supports ATP production in the primitive hematopoietic fraction. By contrast, LSK cells deficient in VHL, an E3 ubiquitin ligase targeting HIF-1α (Semenza, 2010), showed significantly reduced mitochondrial volume compared to wild-type LSK cells (Figure S3B). Because normal quiescent HSCs have relatively little cytoplasm and contain few inactive mitochondria (Kim et al., 1998) (Figure 3G), the decreased mitochondrial mass seen in *VHL*$^{\Delta/\Delta}$ LSK cells suggests that active regulatory mechanisms function in HIF-1α dose-dependent energy production in primitive hematopoietic cells.

HIF-1α Maintains Pdk Expression, Glycolysis, and Transplantation Capacity in LT-HSCs

The decreased glycolysis and activated mitochondrial energy metabolism seen in *HIF-1α*$^{\Delta/\Delta}$ LT-HSCs (Figure 3) suggest that HIF-1α-dependent remodeling of metabolic pathways by Pdk-mediated antagonism of PDH activity occurs in LT-HSCs. Notably, among Pdk family members, *Pdk2* and *Pdk4* mRNA levels were positively correlated with HIF-1α expression in LT-HSCs (Figure 4A). Their mRNA levels decreased in the case of HIF-1α deficiency and increased in the presence of VHL deficiency (Figure 4A). Increased Pdk mRNA levels were suppressed by deletion of both HIF-1α and VHL (Figure 4A). Exposure of LT-HSCs to hypoxia increased expression of Pdk4 but not Pdk2 (Figure S4A), suggesting oxygen-dependent and -independent roles for HIF-1α for the expression of these two genes. To verify that Pdks function as HIF-1α effectors in HSC maintenance, we transduced LT-HSCs or LSK cells with retrovirus expressing Pdk2 or Pdk4 (Figures 4B and S4B). Pdk misexpression (at mRNA levels 100- to 1,000-fold greater than normal) by retrovirus-restored phosphorylation of the PDH-E1α subunit in *HIF-1α*$^{\Delta/\Delta}$ LT-HSCs (Figure 4C) and glycolytic activity in *HIF-1α*$^{\Delta/\Delta}$ LSK cells, as measured by LDH activity (Figure 4D), and antagonized increased mitochondrial ROS generation seen under HIF-1α deficiency (Takubo et al., 2010) (Figure S4D). The number of $Ki67^+$ cycling cells also decreased in Pdk-transduced *HIF-1α*$^{\Delta/\Delta}$ LSK cells (Figure 4E). For in vitro analysis of HSCs, we utilized the SLAM marker to detect HSCs in the LSK population because some LT-HSCs tend to express CD34 in vitro (Noda et al., 2008). *HIF-1α*$^{\Delta/\Delta}$ cells cultured in hypoxic conditions could not sustain an LT-HSC fraction, a deficiency rescued by the introduction of Pdk2 or Pdk4 into *HIF-1α*$^{\Delta/\Delta}$ LSK cells (Figures 4F and 4G).

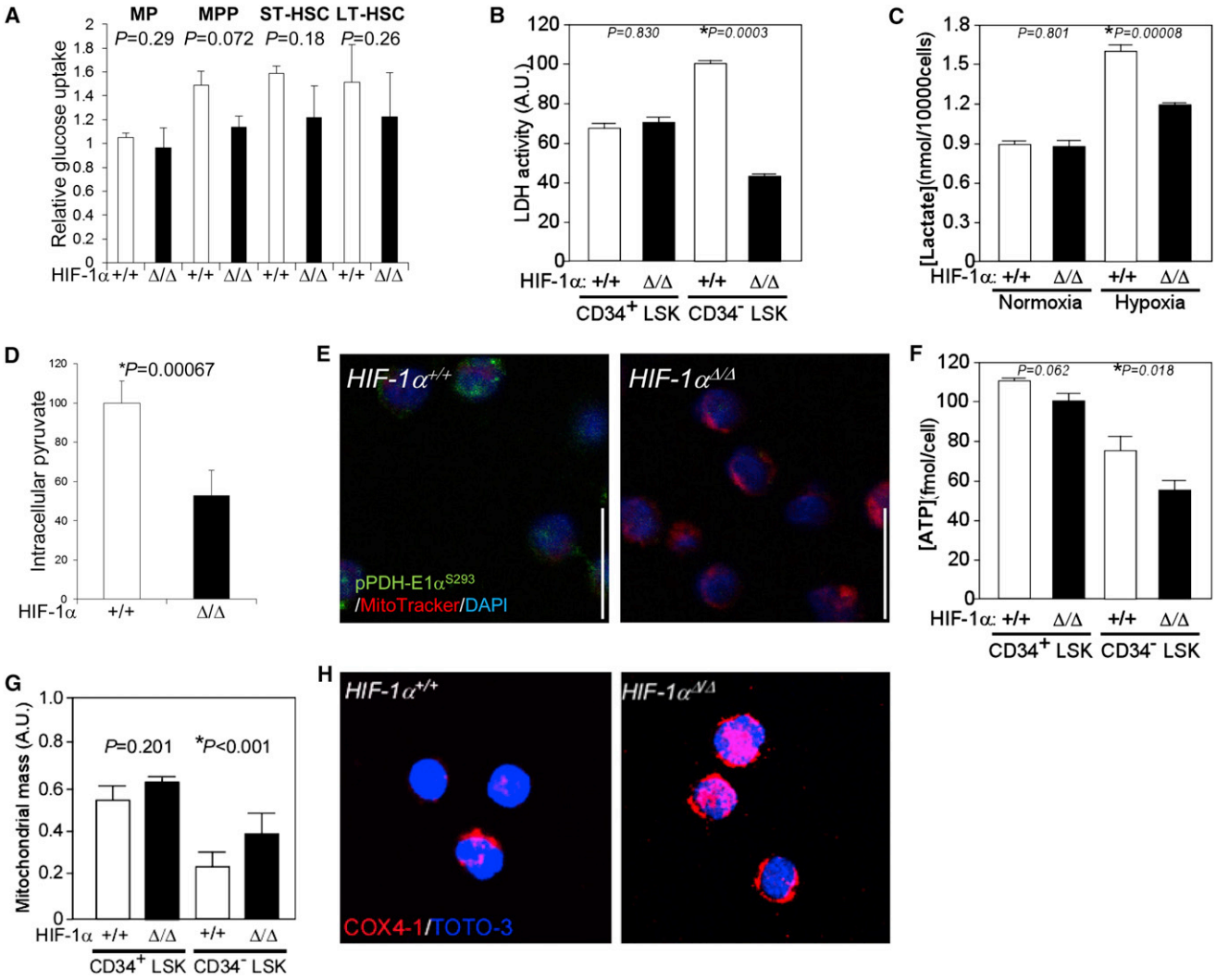

Figure 3. Loss of HIF-1α Alters HSC Energy Metabolism

(A) Relative glucose uptake by LT-HSC, ST-HSC, MPP, and MP cells from *HIF-1α*$^{+/+}$ or *HIF-1α*$^{\Delta/\Delta}$ mice (mean ± SD, n = 4).

(B) LDH activity in CD34$^+$ or CD34$^-$ LSK cells from *HIF-1α*$^{+/+}$ or *HIF-1α*$^{\Delta/\Delta}$ mice (mean ± SD, n = 4). Arbitrary units (a.u.) were calculated as the value relative to LDH activity in the *HIF-1α*$^{+/+}$ CD34$^-$ LSK fraction (set to 100; *p < 0.01).

(C) Lactate production in CD34$^-$ LSK cells under normoxic (20% O_2) or hypoxic (1% O_2) conditions per ten thousand cells (mean ± SD, n = 4; *p < 0.01).

(D) Relative intracellular pyruvate concentrations in LT-HSCs from *HIF-1α*$^{+/+}$ or *HIF-1α*$^{\Delta/\Delta}$ mice (mean ± SD, n = 4; *p < 0.01).

(E) Immunocytochemical staining for phosphorylated S293 residues of PDH-E1α (green), mitochondrial dye Mitotracker DeepRed (red), and DAPI (blue) in *HIF-1α*$^{+/+}$ or *HIF-1α*$^{\Delta/\Delta}$ LT-HSCs.

(F) Intracellular ATP concentration in CD34$^+$ or CD34$^-$ LSK cells from *HIF-1α*$^{+/+}$ or *HIF-1α*$^{\Delta/\Delta}$ mice (mean ± SD, n = 3; *p < 0.05).

(G) Relative mitochondrial mass (mitochondrial fluorescence/nuclear fluorescence) in individual *HIF-1α*$^{\Delta/\Delta}$ CD34$^+$ or CD34$^-$ LSK cells (n = 50). Data are presented as the mean ± SD (*p < 0.001).

(H) Immunocytochemical staining of CD34$^-$ LSK cells for COX4-1 (red) and TOTO-3 (blue).

See also Figure S3.

To test reconstitution capacity, we transplanted 3,000 GFP$^+$-*HIF-1α*$^{\Delta/\Delta}$ LSK cells into lethally irradiated Ly5.1 (CD45.1$^+$) congenic mice together with competitor BM (CD45.1$^+$). Transduced LSK cells in every group contained a similar number of LT-HSCs, as assessed by flow cytometry (data not shown). Twelve weeks after BM transplantation (BMT), *HIF-1α*$^{\Delta/\Delta}$ LSK cells transduced with GFP virus showed significantly decreased repopulation capacity, probably due to upregulation of p16^{Ink4a}/p19^{Arf} in *HIF-1α*$^{\Delta/\Delta}$ LT-HSCs during transduction stress, as previously reported (Takubo et al., 2010). In contrast, *HIF-1α*$^{\Delta/\Delta}$ LSK cells transduced with either Pdk2 or Pdk4 virus showed substantial chimerism and multilineage reconstitution capacity in peripheral blood (PB) compared to control *HIF-1α*$^{\Delta/\Delta}$ cells (Figure 4H and Figure S4E). These experiments suggest that HIF-1α maintains substantial chimerism and multilineage reconstitution capacity through upregulation of Pdk2 and Pdk4 despite expression of other HIF-α family members (Figure S4C).

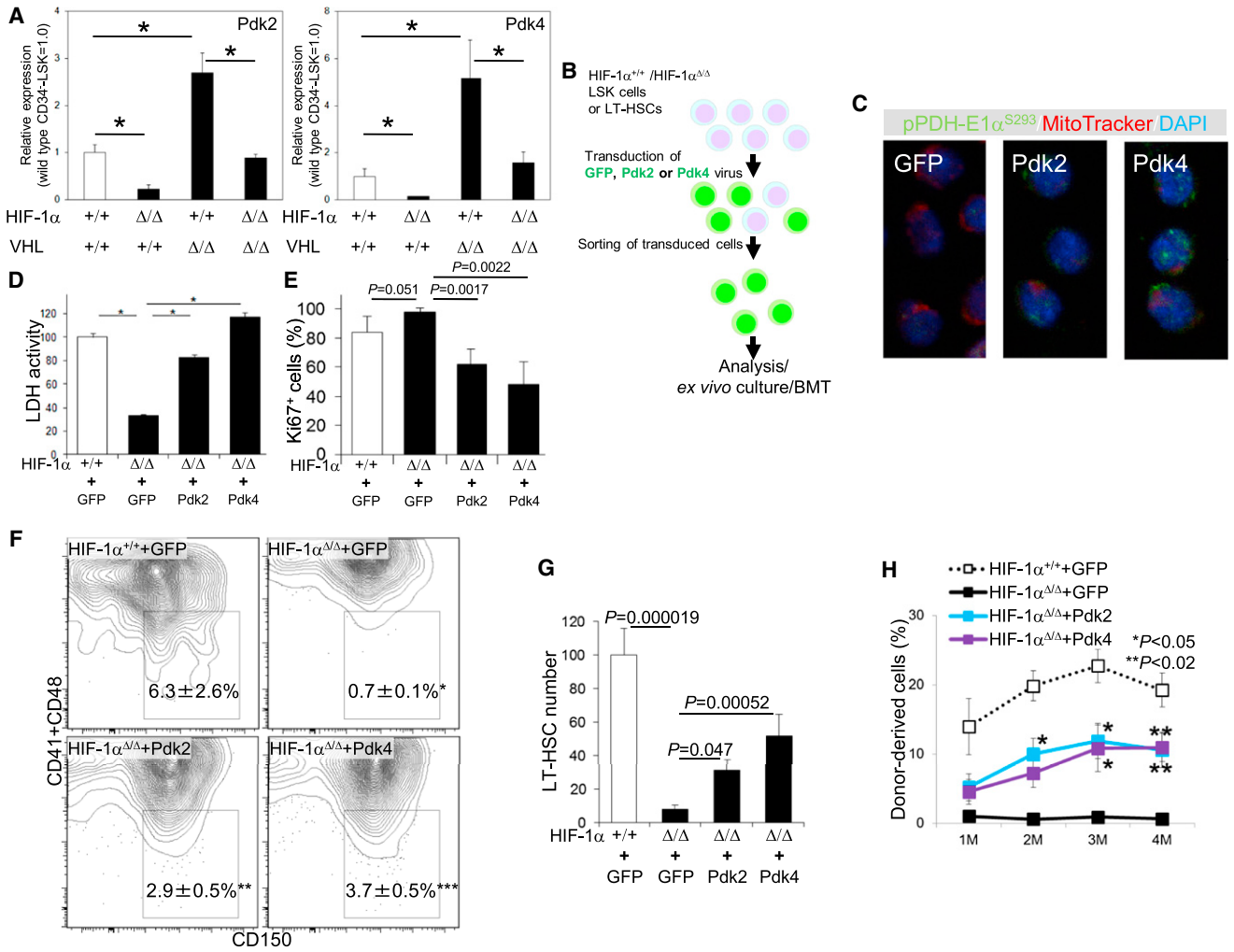

Figure 4. HIF-1α Maintains Pdk Expression, Glycolysis, and Transplantation Capacity in HSCs

(A) qPCR analysis of Pdk2 and Pdk4 expression in the LT-HSC fraction of 12-week-old *HIF-1α*$^{+/+}$, *HIF-1α*$^{Δ/Δ}$, *VHL*$^{Δ/Δ}$ BM, or *HIF-1α*$^{Δ/Δ}$:*VHL*$^{Δ/Δ}$ BM mice (n = 4). Values are normalized to β-actin expression and expressed as fold induction compared to levels detected in *HIF-1α*$^{+/+}$ samples (mean ± SD, n = 4, *p < 0.01).

(B) Design of retroviral rescue of Pdk expression in *HIF-1α*$^{Δ/Δ}$ LSK cells.

(C) Immunocytochemical staining for phosphorylated S293 residues of PDH-E1α (green), Mitotracker DeepRed (red), and DAPI (blue) in *HIF-1α*$^{Δ/Δ}$ LT-HSCs transduced with GFP, Pdk2, or Pdk4 retroviruses.

(D) Intracellular LDH activity in GFP virus-transduced *HIF-1α*$^{+/+}$ LSK cells or in *HIF-1α*$^{Δ/Δ}$ LSK cells transduced with GFP, Pdk2, or Pdk4 retroviruses (mean ± SD, n = 5, *p < 0.000001).

(E) Immunocytochemical assessment of Ki67^{+} in LSK cells transduced with Pdks for 48 hr on a *HIF-1α*$^{+/+}$ or *HIF-1α*$^{Δ/Δ}$ background (mean ± SD, n = 5).

(F) CD150^{+}CD41^{-}CD48^{-} LSK cells after transduction with GFP, Pdk2, or Pdk4 retroviruses and then 7 days of culture under hypoxia (mean ± SD, n = 3, *p < 0.05).

(G) Quantification of total cell number of CD150^{+}CD41^{-}CD48^{-} LSK cells analyzed in (F).

(H) PB chimerism of *HIF-1α*$^{Δ/Δ}$ donor cells transduced with Pdk viruses at 1, 2, 3 and 4 months (M) after BMT (mean ± SEM, n = 5, *p < 0.05, **p < 0.02; compared to *HIF-1α*$^{Δ/Δ}$+GFP virus).

See also Figure S4.

Pdk2 and Pdk4 Are Essential for LT-HSC Transplantation Capacity

To assess whether Pdk functions in LT-HSC maintenance downstream of HIF-1α, we examined hematopoiesis of Pdk2/Pdk4 double knockout mice (Dunford et al., 2011; Jeoung et al., 2006). Peripheral blood counts indicated that these *Pdk2*$^{-/-}$*: Pdk4*$^{-/-}$ mice were mildly but significantly anemic compared to control mice (Figure 5A). Various populations of differentiated and undifferentiated cells in the BM, spleen, and thymus were unchanged in number in *Pdk2*$^{-/-}$*: Pdk4*$^{-/-}$ mice (Figures S5A–S5E). Progenitor capacity of *Pdk2*$^{-/-}$*: Pdk4*$^{-/-}$ LSK cells, as assessed by the colony-forming capacity in semi-solid methylcellulose plus cytokines, was identical to that of control cells (Figure 5B), suggesting that steady-state hematopoiesis and progenitor capacity is maintained in *Pdk2*$^{-/-}$*: Pdk4*$^{-/-}$ mice. To investigate self-renewal and multilineage differentiation capacity of *Pdk2*$^{-/-}$*: Pdk4*$^{-/-}$ LT-HSCs, we performed BM transplantation of these cells with congenic

A

	Control	*Pdk2*$^{-/-}$:*Pdk4*$^{-/-}$	P value
WBC(/ul)	11429±3259	10000±4320	0.498
RBC(x10^4/ul)	1019±34	1007±41	0.583
Hb(g/dl)	15.9±0.4	15.0±0.0	<0.001
HCT(%)	51.3±1.3	49.6±1.0	0.014
MCV(fl)	50.4±1.4	49.3±1.7	0.206
MCH(pg)	15.6±0.4	14.9±0.6	0.043
Plt(x10^4/ul)	88.4±27.4	82.0±36.4	0.716

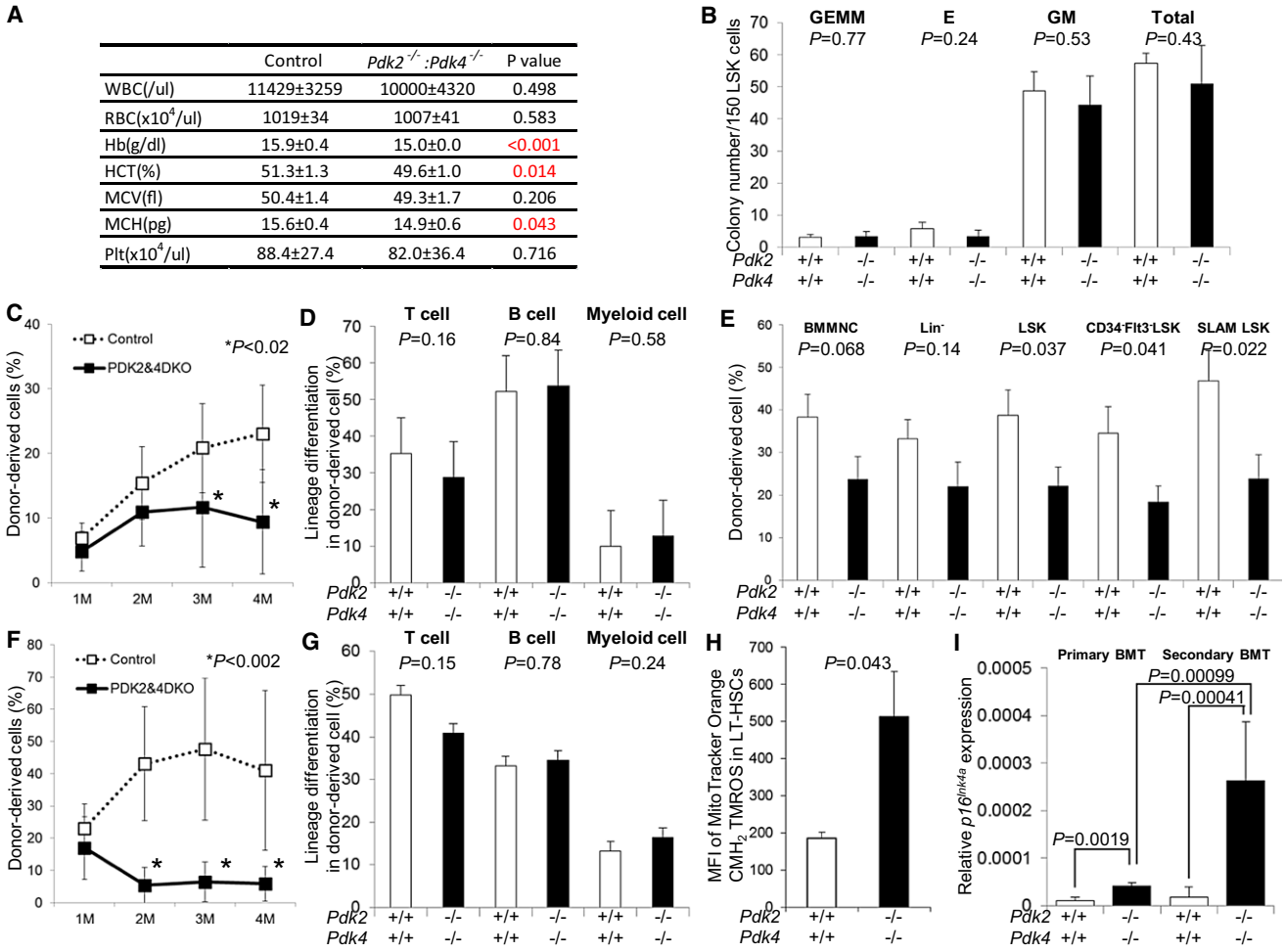

Figure 5. Defective Maintenance of *Pdk2*$^{-/-}$: *Pdk4*$^{-/-}$ HSCs after Transplantation

(A) PB counts in control and *Pdk2*$^{-/-}$: *Pdk4*$^{-/-}$ mice (mean ± SD, n = 7).

(B) Colony-forming capacity of control (open bars) and *Pdk2*$^{-/-}$: *Pdk4*$^{-/-}$ LSK cells (closed bars) (mean ± SD, n = 3). CFU-GEMM, CFU-E, CFU-GM, and total colony numbers are indicated.

(C) PB chimerism in primary BMT recipients of control (open boxes) or *Pdk2*$^{-/-}$: *Pdk4*$^{-/-}$ LT-HSC (closed boxes) cells at 1, 2, 3 and 4 months (M) after BMT (mean ± SD, n = 10).

(D) Differentiation status (CD4/CD8+ T cells, B220+ B cells, or Mac-1/Gr-1+ myeloid cells) of donor-derived (Ly5.2+) PB cells in primary BMT recipients of control (open bars) or *Pdk2*$^{-/-}$: *Pdk4*$^{-/-}$ (closed bars) LT-HSCs (mean ± SD, n = 10).

(E) Donor-derived (Ly5.2+) BM MNC, Lin$^-$, LSK, CD34$^-$Flt3$^-$ LSK, or SLAM-LSK chimerism in primary BMT recipients of control (open bars) or *Pdk2*$^{-/-}$: *Pdk4*$^{-/-}$ (closed bars) LT-HSCs 4 months after primary BMT (mean ± SEM, n = 10).

(F) PB chimerism in secondary recipients of BM derived from primary recipients of control (open boxes) or *Pdk2*$^{-/-}$: *Pdk4*$^{-/-}$ (closed boxes) MNCs, at indicated times after BMT (mean ± SD, n = 10).

(G) Differentiation status (CD4/CD8+ T cells, B220+ B cells, or Mac-1/Gr-1+ myeloid cells) of donor-derived (Ly5.2+) PB cells in secondary BMT recipients of control (open bars) or *Pdk2*$^{-/-}$: *Pdk4*$^{-/-}$ (closed bars) cells (mean ± SD, n = 10).

(H) Redox-sensitive MitoTracker fluorescence in control (open bars) or *Pdk2*$^{-/-}$: *Pdk4*$^{-/-}$ (closed bars) BM LT-HSCs (n = 3, mean ± SD).

(I) Quantitative PCR analysis of p16^{Ink4a} expression in control (open bars) or *Pdk2*$^{-/-}$: *Pdk4*$^{-/-}$ (closed bars) donor-derived LT-HSCs 4 months after primary BMT (n = 4). Values are normalized to β-actin expression and expressed as fold induction compared to levels detected in *HIF-1α*$^{+/+}$ Ly5.2$^+$ LSK samples (mean ± SD).

See also Figure S5.

competitors into lethally irradiated recipient mice. In contrast to the capacity of differentiated counterparts, LT-HSCs were defective in repopulation of primary recipient peripheral blood at 3–4 months after transplantation (Figure 5C). Four months after BMT, *Pdk2*$^{-/-}$: *Pdk4*$^{-/-}$ donor-derived cells retained differentiation capacity of T, B, and myeloid cells comparable with control donor-derived cells (Figure 5D). At that time, recipients of *Pdk2*$^{-/-}$: *Pdk4*$^{-/-}$ donor cells exhibited less chimerism than did recipients of control donor cells in the LSK-gated, CD34$^-$Flt3$^-$ LSK-gated, or SLAM-LSK-gated fraction of BM (Figure 5E), indicating that HSC levels decreased. We then isolated and transplanted 1 × 10^6 primary donor-derived MNCs into secondary recipients. We observed a clear defect in long-term reconstitution ability of *Pdk2*$^{-/-}$: *Pdk4*$^{-/-}$

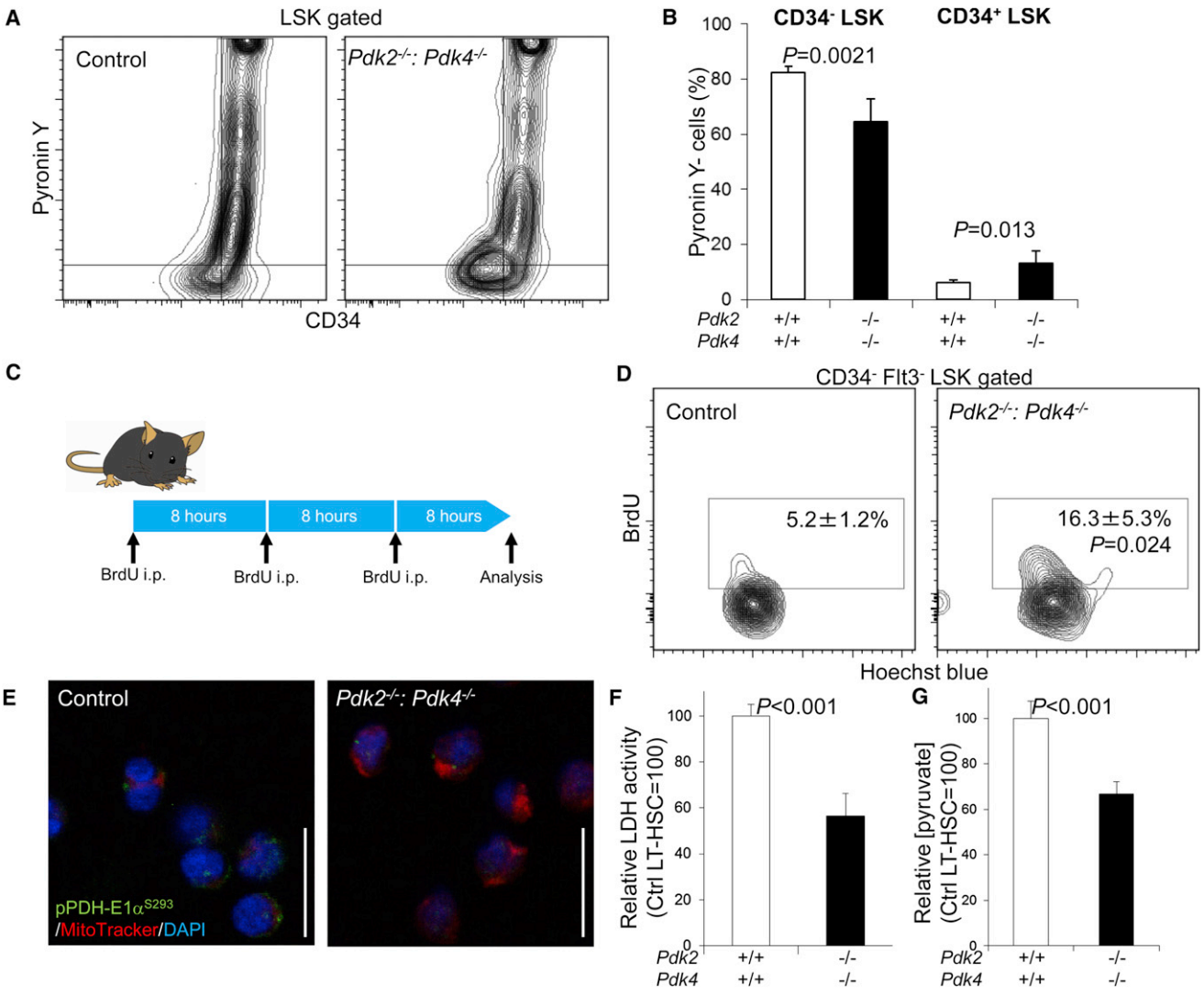

Figure 6. Loss of Cell Cycle Quiescence and Glycolytic Capacity in *Pdk2*$^{-/-}$: *Pdk4*$^{-/-}$ HSCs

(A) Representative flow cytometric plot of Pyronin Y analysis in the LSK-gated fraction of control or *Pdk2*$^{-/-}$: *Pdk4*$^{-/-}$ BM MNCs.

(B) Summary of flow cytometric Pyronin Y analysis of CD34^{-} LSK or CD34^{+} LSK fractions in control or *Pdk2*$^{-/-}$: *Pdk4*$^{-/-}$ BM MNCs (mean ± SD, n = 6).

(C) Design of short-term BrdU labeling assay in control or *Pdk2*$^{-/-}$: *Pdk4*$^{-/-}$ mice.

(D) Representative flow cytometric plot showing BrdU labeling of the LT-HSC-gated fraction from control or *Pdk2*$^{-/-}$: *Pdk4*$^{-/-}$ BM MNCs. Numbers indicate the frequency of the BrdU+ fraction in LT-HSCs (mean ± SD, n = 3).

(E) Immunocytochemical staining for the phosphorylated S293 residue of PDH-E1α (green), Mitotracker DeepRed (red), and DAPI (blue) in control or *Pdk2*$^{-/-}$: *Pdk4*$^{-/-}$ LT-HSCs.

(F) LDH activity in LT-HSCs from control or *Pdk2*$^{-/-}$: *Pdk4*$^{-/-}$ mice (mean ± SD, n = 4). Shown are arbitrary values calculated as the value relative to LDH activity in the control LT-HSC fraction (set to 100).

(G) Intracellular pyruvate concentration in LT-HSCs from control or *Pdk2*$^{-/-}$: *Pdk4*$^{-/-}$ mice (mean ± SD, n = 3). Shown are arbitrary values calculated as the value relative to intracellular pyruvate levels in the control LT-HSC fraction (set to 100).

See also Figure S6.

HSCs in the PB and BM of secondary recipients (Figures 5F and S5F) without any differentiation defect 4 months after secondary transplantation (Figure 5G). We isolated and transplanted 1 × 10^6 secondary donor-derived MNCs into tertiary recipients. We observed no long-term reconstitution ability of *Pdk2*$^{-/-}$: *Pdk4*$^{-/-}$ HSCs in the PB of tertiary recipients (Figure S5G). ROS reportedly induces p16^{Ink4a} expression (Takahashi et al., 2006), and p16^{Ink4a} enhances HSC aging (Janzen et al., 2006). We observed increased mitochondrial ROS production in *Pdk2*$^{-/-}$: *Pdk4*$^{-/-}$ LT-HSCs (Figure 5H). Thus, ROS-mediated senescence of *Pdk2*$^{-/-}$: *Pdk4*$^{-/-}$ LT-HSCs could account for loss of stem cell properties through p16^{Ink4a} upregulation. In support of this idea, we detected significantly elevated levels of p16^{Ink4a} transcripts in *Pdk2*$^{-/-}$: *Pdk4*$^{-/-}$ LT-HSCs from primary and secondary BMT recipients (Figure 5I).

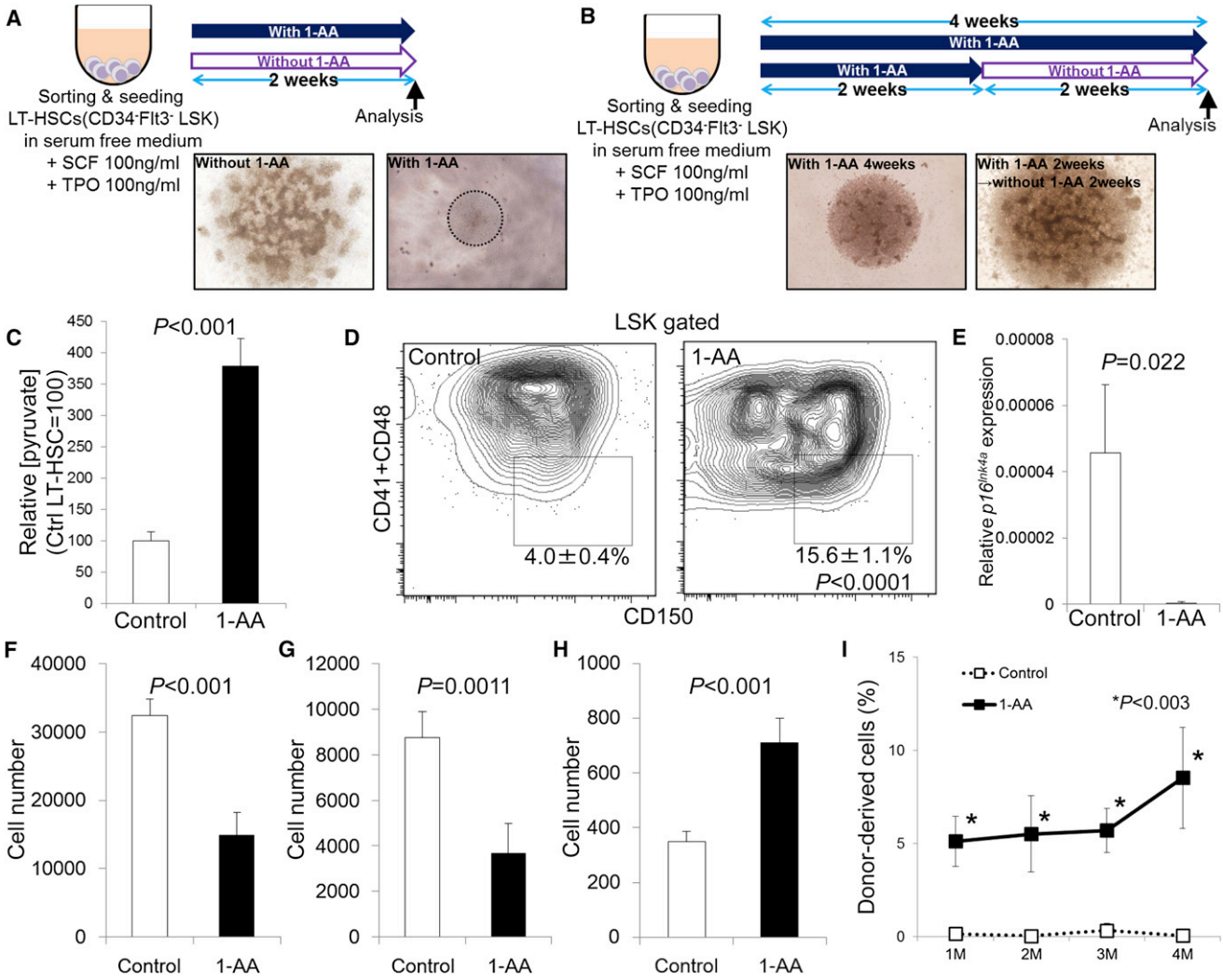

Figure 7. Modulation of HSC Cell Cycle Quiescence by a PDH Inhibitor

(A) Design of LT-HSC cultures treated with or without 1-AA for 2 weeks. Light microscopic data show colony morphology.

(B) Effect of 1-AA withdrawal on LT-HSCs after 2 weeks of treatment. Light microscopic colony morphology after 4 weeks of culture.

(C) Intracellular pyruvate concentrations in LT-HSCs treated with or without 1-AA for 4 days (mean ± SD, n = 3). Shown are arbitrary values calculated as the value relative to intracellular pyruvate in the control LT-HSC fraction (set to 100).

(D) Flow cytometric analysis of LT-HSCs treated with or without 1-AA in vitro for 4 weeks. Numbers indicate the LT-HSC fraction in LSK cells (mean ± SD, n = 4).

(E) Quantitative PCR analysis of $p16^{Ink4a}$ expression in control (open bars) or 1-AA-treated (closed bars) LT-HSCs 2 weeks after culture with or without 1-AA (n = 4). Values are normalized to β-actin expression and expressed as fold induction compared to levels detected in control samples (mean ± SD).

(F–H) Quantification of total cells (F), LSK cells (G), or LT-HSCs (H) from LT-HSC-derived colonies in the absence (control) or presence of 1-AA for 4 weeks in vitro (mean ± SD, n = 4).

(I) Donor-derived ($Ly5.1^+$) PB chimerism in BMT recipients of control LT-HSCs or LT-HSCs treated with 1-AA for 4 weeks, at indicated times after BMT (mean ± SD, n = 4–5).

See also Figure S7.

Pdks Are Essential for LT-HSC Cell Cycle Quiescence and Metabolism

The pivotal role played by Pdk2 and Pdk4 in LT-HSC senescence during transplantation suggests that Pdk-mediated antagonism of mitochondrial metabolism prevents LT-HSC senescence by maintaining cell cycle quiescence. To test this hypothesis, we examined cell cycle kinetics of the $Pdk2^{-/-}$: $Pdk4^{-/-}$ LT-HSCs by multicolor flow cytometry. Although the number of LT-HSCs, ST-HSCs, and MPPs was unchanged in $Pdk2^{-/-}$: $Pdk4^{-/-}$ mice (Figures S5D and S5E), we detected specific activation of the cell cycle, characterized by a reduction in the Pyronin Y^- G0 fraction and an increase in the Pyronin Y^+ G1 fraction, in $Pdk2^{-/-}$: $Pdk4^{-/-}$ $CD34^-$ LSK cells (Figures 6A and 6B). Recipient mice whose BM was replaced by $Pdk2^{-/-}$: $Pdk4^{-/-}$ MNCs ($Pdk2^{-/-}$: $Pdk4^{-/-}$ BM mice) also showed similar loss of the G0 fraction in $Pdk2^{-/-}$: $Pdk4^{-/-}$ $CD34^-$ LSK cells (Figures S6A and S6B). Interestingly, $CD34^+$ LSK cells showed an increase in the Pyronin Y^- G0 fraction in $Pdk2^{-/-}$: $Pdk4^{-/-}$ mice (both

hematopoietic cells and hematopoietic microenvironment are *Pdk2*$^{-/-}$: *Pdk4*$^{-/-}$), but not in *Pdk2*$^{-/-}$: *Pdk4*$^{-/-}$ BM mice (*Pdk2*$^{-/-}$: *Pdk4*$^{-/-}$ hematopoietic cells and *Pdk2*$^{+/+}$: *Pdk4*$^{+/+}$ hematopoietic microenvironment) (Figures 6A, 6B, S6A, and S6B). These observations suggest that *Pdk2*$^{-/-}$: *Pdk4*$^{-/-}$ nonhematopoietic cells limit blood cell production by slowing the G0/G1 progression of *Pdk2*$^{-/-}$: *Pdk4*$^{-/-}$ progenitors. Also, short-term BrdU labeling indicated high levels of cycling cells in the *Pdk2*$^{-/-}$: *Pdk4*$^{-/-}$ LT-HSC population (Figures 6C and 6D). In addition to the cell cycle defect, we detected metabolic defects in *Pdk2*$^{-/-}$: *Pdk4*$^{-/-}$ mice. In *Pdk2*$^{-/-}$: *Pdk4*$^{-/-}$ LT-HSCs, PDH-E1α subunit phosphorylation status was decreased (Figures 6E, S6C, and S6D) and intracellular LDH activity and pyruvate content were significantly attenuated (Figures 6F and 6G). These findings indicate that Pdks are necessary to maintain cell cycle quiescence and LT-HSC metabolic properties.

A Pdk Mimetic Modulates Cell Cycle Quiescence in LT-HSCs

To determine whether metabolic reprogramming could be achieved in HSCs, we artificially suppressed PDH activity using the PDH inhibitor, 1-aminoethylphosphinic acid (1-AA). This molecule is converted by aminotransferase to the pyruvate analog acetylphosphinic acid, which competes with pyruvate to suppress PDH enzymatic activity (Laber and Amrhein, 1987; Nemeria et al., 2006). In vitro treatment of isolated LT-HSCs, ST-HSCs, or MPPs with or without 1-AA for 2 weeks maintained LT-HSCs and ST-HSCs (Figures 7A, S7A, and S7B). No viable cells were detected in MPPs in the presence of 1-AA after 2 weeks of culture (Figure S7B). Colony growth of LT- or ST-HSCs in the culture medium was suppressed by 1-AA in vitro (Figure S7B). LT-HSCs cultured with 1-AA for 2 weeks could proliferate again after removal of 1-AA (Figure 7B). Treatment of LT-HSCs with 1-AA in vitro showed higher pyruvate levels than nontreated LT-HSCs (Figure 7C). In vitro treatment of isolated LT-HSCs, ST-HSCs, or MPPs with or without 1-AA for 4 weeks only maintained LT-HSCs (Figure S7C). No viable cells were detected in ST-HSCs and MPPs in the presence of 1-AA after 4 weeks of culture (Figures S7A and S7C). Colony growth of LT-HSCs in the culture medium was suppressed by 1-AA in vitro (Figure S7C). Flow cytometric analysis of LT-HSC-derived colony after 4 weeks of culture revealed preferential maintenance of LT-HSC frequency within LSK cells in the presence of 1-AA compared to control cells (Figure 7D). LT-HSCs treated with 1-AA for 2 weeks lacked expression of p16^{Ink4a} mRNA in LT-HSCs (Figure 7E). Both the total number of cells and that of LSK cells were suppressed by 1-AA treatment after 4 weeks of culture (Figures 7F and 7G). In contrast, 1-AA treatment maintained the LT-HSC fraction in vitro (Figure 7H). Transplanted LT-HSC-derived colonies after 4 weeks of culture retained reconstitution capacity of PB and BM during transplantation (Figures 7I and S7D). These data collectively suggest that metabolic reprogramming by Pdk induction could be a potent tool to modulate the cell cycle of LT-HSCs.

DISCUSSION

The present study provides direct evidence for metabolic specificity of LT-HSCs compared to progenitors or terminally differentiated cells. Our observations indicate that LT-HSCs specifically activate glycolysis and suppress influx of glycolytic metabolites into mitochondria via Pdk activity. We also demonstrate the importance of glycolytic ATP production promoted by the HIF-1α/Pdk regulatory system for HSC stem cell capacity by maintaining cell cycle quiescence. In lower eukaryotes, quiescence is defined not only in terms of the cell cycle but as a metabolically specific state characterized by suppressed catabolism and resulting in a nondividing phase (Allen et al., 2006; Klosinska et al., 2011; Laporte et al., 2011). Establishment of cell cycle quiescence via altered metabolic activity is an effective strategy to survive extreme conditions of starvation or hypoxia.

Our initial metabolomics analysis of purified HSCs, progenitors, and terminally differentiated cells using CE-TOFMS indicated that quiescent LT-HSCs exhibit specific carbon metabolism phenotypes favoring glycolysis (Figures 1A and S1A). Low ATP levels generated in LSK fraction subpopulations, which are maintained by glycolysis, gradually increase during differentiation from LT-HSCs to MPPs through ST-HSCs (Figure 1B). Likewise, various glycolytic regulators are highly expressed in LT-HSCs in a HIF-1α-dependent manner. Among these regulators, levels of Pdk2 and Pdk4 are regulated by HIF-1α levels. Pdk actively suppresses mitochondrial metabolism and maintains ATP generation during hypoxia through PDH-E1α phosphorylation (Harris et al., 2002). Pdk1 is reportedly a direct HIF-1α target in murine embryonic fibroblasts and human solid tumor cell lines (Kim et al., 2006; Papandreou et al., 2006). Our data suggest that Pdk2 and Pdk4 are downstream effectors of HIF-1α in maintaining LT-HSC cell cycle quiescence. Rescue of *HIF-1α*$^{\Delta/\Delta}$ HSCs by Pdk overexpression as well as loss-of-function experiments in HSCs from *Pdk2*$^{-/-}$: *Pdk4*$^{-/-}$ mice indicate an important role for Pdks on LT-HSC cell cycle quiescence in a HIF-1α-dependent manner. Therefore, Pdk probably functions in two ways, via activation of glycolysis and suppression of influx of glycolytic metabolites into mitochondria, to maintain LT-HSCs in a hypoxic, hypoperfused, and low-nutrient niche in the BM. Metabolic activities demonstrated here may also protect HSCs from ROS generation either through mitochondria or through accelerated consumption of NADH by LDH activity, which would ameliorate oxidative stress (Suematsu et al., 1992). In addition, products of the TCA cycle, including citrate, could return to the cytosol to drive lipid metabolism required for cell growth and proliferation (Lum et al., 2007). Thus, Pdk could suppress mitochondrial ROS generation and decrease the lipid supply to modulate cellular proliferation. The characteristic metabolite pool in LT-HSCs may also activate a signaling pathway favoring quiescence. Because the Pdk mimetic 1-AA induced increased levels of pyruvate and enhanced LT-HSC maintenance via cell cycle quiescence in vitro, suppression of glycolytic metabolic influx into mitochondria and activation of glycolysis via the HIF-1α/Pdk system could be the primary event in generating HSC quiescence. Activation of a Pdk/PDH checkpoint results in a decoupling of glycolysis and the mitochondrial TCA cycle and might confer a metabolic robustness through two independent energy factories—glycolysis and TCA cycle—in LT-HSCs. Although 1-AA induced ST-HSC cell cycle suppression and maintained cells for 2 weeks, they died in vitro after 4 weeks in culture. Therefore, cell cycle suppression via the PDH may function not only in LT-HSCs but also in differentiated ST-HSCs, although additional

metabolic programs may also maintain ST-HSCs. In addition, 1-AA treatment not only supported the cell number of LT-HSCs but also had a qualitative effect on transplantation capacity of LT-HSCs, as shown in Figures 7I and S7D. Overall, suppression of mitochondrial metabolite flux by Pdks is an efficient strategy for stem cell maintenance. This observation is in contrast to the activity of cancer cells, which utilize aerobic glycolysis and suppress mitochondrial metabolism to promote proliferation rather than quiescence (DeBerardinis et al., 2008; Jones and Thompson, 2009). Thus, the existence of differing molecular mechanisms underlying identical metabolic phenotypes may suggest strategies for novel tumor-specific therapy.

Although we could rule out the importance of other Pdks, including Pdk1 and Pdk3, on *HIF-1α*$^{\Delta/\Delta}$ HSCs, it is noteworthy that *HIF-1α*$^{\Delta/\Delta}$ LT-HSCs, which show decreased Pdk2/4 expression, exhibit decreased phosphorylation of PDH-E1α and increased mitochondrial size. These size changes may be due to HIF-1α-regulated increases in mitochondrial biogenesis (Zhang et al., 2007) or reduced mitochondrial autophagy (Zhang et al., 2008). However, reduced ATP content resulting from attenuated glycolysis, a hallmark of senescent cells (Zwerschke et al., 2003), seen in *HIF-1α*$^{\Delta/\Delta}$ LT-HSCs could not be rescued by mitochondrial ATP generation (Figure 3F), suggesting an essential role for anaerobic glycolysis in energy production by hypoxic HSCs. Because *VHL*$^{\Delta/\Delta}$ LSK cells show decreased mitochondrial content, mitochondrial mass is probably also regulated by the VHL/HIF-1α regulatory system in HSCs and progenitors. Various studies of HSCs defective in ATP generation indicate that LT-HSCs exhibit mitochondrial defects (Liu et al., 2009; Nakada et al., 2010; Gurumurthy et al., 2010; Gan et al., 2010; Sahin et al., 2011). Therefore, although influx of glycolytic metabolites into mitochondria is suppressed by Pdks, mitochondrial metabolic integrity is apparently important for LT-HSC maintenance. The elucidation of these integrative metabolic programs in LT-HSCs extends the concept of the stem cell niche and suggests a strategy for maintaining and expanding HSC resources by modulating their quiescence via Pdk/PDH modulators or enhancement of HIF-1α signaling.

EXPERIMENTAL PROCEDURES

CE-TOFMS Analysis

For CE-TOFMS analysis, BM cells including CD34$^-$Flt3$^-$ LSK (LT-HSCs), CD34$^+$Flt3$^-$ LSK (ST-HSCs), CD34$^+$Flt3$^+$ LSK (MPPs), Lin$^-$ c-Kit$^+$ Sca-1$^-$ (MPs), Gr-1/Mac-1+ (myeloid cells), CD4/CD8+ (T cells), and B220+ (B cells) (1–2 × 10^6 cells) sorted from 120 C57BL/6 mice (12 weeks old) were lysed to extract metabolites. Metabolomic profiling and data analysis were performed twice essentially as described (Soga et al., 2003, 2006).

Mice

Mx1-cre:HIF-1α$^{flox/flox}$, *Mx1-cre:VHL*$^{flox/flox}$ or *Pdk2*$^{-/-}$*: Pdk4*$^{-/-}$ mice (Takubo et al., 2010; Dunford et al., 2011; Jeoung et al., 2006) were genotyped using PCR-based assays of tail DNA samples. To prepare *HIF-1α*$^{\Delta/\Delta}$ mice, we induced Mx1-cre expression by intraperitoneal injection of 400 μg of pIpC (Amersham or Sigma) into 4- to 8-week-old mice on 3 alternate days. Age-matched pIpC-injected *Mx1-cre:HIF-1α*$^{+/+}$ mice or *Cre(-):HIF-1α*$^{flox/flox}$ mice served as controls (*HIF-1α*$^{+/+}$ mice). C57BL/6-Ly5.1 congenic or C57BL/6-Ly5.1/Ly5.2 F1 mice were used for competitive repopulation assays. To prepare mice with *VHL*$^{\Delta/\Delta}$, *HIF-1α*$^{\Delta/\Delta}$*:VHL*$^{\Delta/\Delta}$ or *Pdk2*$^{-/-}$*: Pdk4*$^{-/-}$ BM (*VHL*$^{\Delta/\Delta}$, *HIF-1α*$^{\Delta/\Delta}$*:VHL*$^{\Delta/\Delta}$ or *Pdk2*$^{-/-}$*: Pdk4*$^{-/-}$ BM mice), we transplanted 6 × 10^6–1 × 10^7 BM MNCs or CD45$^+$ BM MNCs from *Mx1-cre:VHL*$^{flox/flox}$ or *Mx1-cre:HIF-1α*$^{flox/flox}$*: VHL*$^{flox/flox}$ mice into lethally irradiated C57BL/6-Ly5.1 mice. Six weeks after BMT, we checked for peripheral blood chimerism and utilized recipients with more than 90% donor-derived cells. Cre expression in replaced BM was induced by intraperitoneal injection of 250 μg of pIpC (Amersham or Sigma) on 3 alternate days. *Mx1-cre:HIF-1α*$^{+/+}$*:VHL*$^{+/+}$ or *Pdk2*$^{+/+}$*: Pdk4*$^{+/+}$ BM mice served as controls.

Antibodies

The following monoclonal antibodies (mAbs) were used in this study: rat mAbs against c-Kit (2B8), Sca-1 (E13-161.7), CD4 (L3T4), CD8 (53-6.72), B220 (RA3-6B2), TER-119, Gr-1 (RB6-8C5), CD34 (RAM34), Mac-1 (M1/70), CD3 (500A2), Flt-3 (A2F10.1), CD41 (MWReg30), CD48 (HM48-1), CD150 (TC15-12F12.2), CD45.2 (104), and CD45.1 (A20). All rat mAbs were purchased from BD, eBiosciences, or Biolegend. A mixture of mAbs against CD4, CD8, B220, TER-119, Mac-1, and Gr-1 was used as a lineage marker (Lineage). We also utilized anti-Ki67 (SP-6, Labvision), anti-PDH-E1α (pSer293) (Merck), anti-PDH-E1α (pSer300) (Merck), and anti-COX4-1 (MitoSciences) antibodies for immunocytochemical experiments.

Flow Cytometry

Analysis of various HSC fractions, detection of Side Population by Hoechst 33342, and Pyronin Y analysis were performed essentially as described (Arai et al., 2004). For flow cytometry analysis of metabolic properties of quiescent stem cells, we pretreated BM MNCs in vitro with 2-DG and/or NaN_3 10 min before staining with Hoechst 33342. For flow cytometric analysis of glucose uptake, BM cells were isolated and preincubated for 30 min at 37°C with 2-[N-(7-Nitrobenz-2-Oxa-1,3-Diazol-4-yl)Amino]-2-Deoxy-D-Glucose or 2-[N-(7-Nitrobenz-2-Oxa-1,3-Diazol-4-yl)Amino]-2-Deoxy-L-Glucose (negative control) (Peptide Institute) before staining with surface markers. For intracellular flow cytometry analysis of phosphorylated PDH-E1α^{S293}, cells were fixed and permeabilized as previously described (Takubo et al., 2010) and stained with anti-phosphorylated pPDH-E1α^{S293} antibody and a fluorophore-labeled secondary antibody.

Immunocytochemistry

Immunocytochemistry of isolated cells was performed as described (Takubo et al., 2008). In brief, cells were attached to glass slides and fixed with 4% PFA. Slides were then blocked with a protein blocker (DAKO) to avoid nonspecific staining. Specimens were reacted with primary antibodies followed by fluorophore-labeled secondary antibodies and nuclear staining.

Cell Cycle Analysis

For immunocytochemical analysis, Ki67$^+$ cells were detected with an anti-Ki67 antibody (SP-6) followed by incubation with a fluorophore-labeled anti-rabbit Ig antibody (MolecularProbes). The cutoff range for fluorescence was determined by a negative control sample stained with an isotype control Ig followed by secondary Ab treatment. The proportion of Ki67-positive cells in each fraction was determined by counting. At least 500 cells per sample were examined for each specimen. For FACS analysis of the cell cycle, cells were first stained with antibodies for surface markers and then fixed and permeabilized to detect the intracellular BrdU with BrdU Flow Kit (Beckman Coulter).

Analysis of Mitochondrial Mass and ROS Production

For confocal microscopy of mitochondria, sorted cells were stained with anti-COX4-1 antibody or incubated for 30 min at 37°C with 100 nM mitotracker Deep Red (MolecularProbes), which binds to mitochondrial membranes independent of membrane potential. Stained cells were attached to glass slides and counterstained with TOTO-3 or DAPI (MolecularProbes) for 30 min. Samples were then three-dimensionally analyzed by laser confocal microscopy for the relative mitochondrial volume of individual cells under identical acquisition settings in the linear range of the acquired fluorescence. We randomly chose cells in multiple fields (more than five fields per sample). Mitochondrial fluorescence was normalized to nuclear DNA fluorescence. To detect mitochondrial ROS production, we stained sorted cells with 100 nM Mitotracker Orange CMH_2TMROS (MolecularProbes) for 30 min at 37°C and analyzed them by FACS.

Quantitative RT-PCR

Quantitative PCR was performed as described previously (Takubo et al., 2008). The cDNA equivalent of 500 cells per reaction was used as a template

for one PCR reaction. PCR primers for each gene were purchased from TaKaRa Bio.

Virus Transduction

For retrovirus transduction, murine Pdk2 and Pdk4 cDNAs were subcloned upstream of IRES-EGFP in pMY-IRES-EGFP (Nosaka et al., 1999). To produce recombinant retrovirus, we transfected plasmid DNA into Plat-E cells by FuGENE (Roche). Supernatants of transfected cells were used to transduce LSK cells or LT-HSCs precultured with SCF and thrombopoietin (TPO) for 16 hr. At 48 hr posttransduction, GFP^+ cells were sorted by FACS and analyzed, transplanted, or cultured for assays.

Serum-free HSC Culture

Sorted cells were cultured on U-bottomed fibronectin-coated plates. Cultures were maintained in SF-O3 medium (Sanko Junyaku) containing 1.0% BSA, 100 ng/ml SCF, 100 ng/ml TPO with or without 1-AA. After 14 or 28 days of cultivation, cells were collected, stained with fluorophore-labeled mAb, and analyzed by FACS or used for immunocytochemical and metabolic analysis.

Bone Marrow Transplant

For Pdk rescue experiments, transduced GFP^+ LSK cells from *HIF-1*$\alpha^{+/+}$ or *HIF-1*$\alpha^{\Delta/\Delta}$ mice (Ly5.2), together with 4×10^5 BM MNCs from C57BL/6-Ly5.1 mice, were transplanted into lethally irradiated C57BL/6-Ly5.1 congenic mice. For *Pdk2*$^{-/-}$*: Pdk4*$^{-/-}$ mice, 500 $CD34^-Flt3^-$ LSK cells from *Pdk2*$^{+/+}$*: Pdk4*$^{+/+}$ or *Pdk2*$^{-/-}$*: Pdk4*$^{-/-}$ mice (Ly5.2), together with 4×10^5 BM MNCs from C57BL/6-Ly5.1 mice, were transplanted into lethally irradiated C57BL/6-Ly5.1 congenic mice. For 1-AA treatment, 830 $CD34^-Flt3^-$ LSK cells from C57BL/6-Ly5.1 mice were cultured in SF-O3 medium containing 1.0% BSA, 100 ng/ml SCF, 100 ng/ml TPO with or without 1-AA and the colony derived from 830 $CD34^-Flt3^-$ LSK cells at day 28 was harvested and transplanted into lethally irradiated C57BL/6 mice (Ly5.2) with 4×10^5 BM MNCs from C57BL/6 mice. One, two, three, and four months after BMT, peripheral blood was collected and examined to determine the percentage of donor-derived cells and the differentiation status of donor-derived cells by FACS. Four months after BMT, BM MNCs were collected and examined to determine the percentage of donor-derived cells by FACS.

Determination of Intracellular ATP, LDH Activity, Pyruvate Content, and PK Activity

Sorted cells ($1–5 \times 10^4$) were lysed, and intracellular ATP, LDH activity, pyruvate content, or PK activity was measured using the Luciferase ATP Determination Kit (Sigma), the LDH Cytotoxicity Detection Kit (TaKaRa), the Pyruvate Assay Kit (BioVision), or the Pyruvate Kinase Activity Assay Kit (BioVision), respectively, following the manufacturers' instructions.

OCR Determination

Sorted cells (5×10^4) were attached to the bottom of a XF96 Tissue Culture Plate (Seahorse Bioscience) coated with BD Cell-Tak Cell Adhesive. Then, cells were incubated in the presence of SCF and TPO with or without oligomycin and OCR was measured by XF96 Extracellular Flux Analyzer (Seahorse Bioscience).

Analysis of HSC Lactate Production

Sorted cells ($1–5 \times 10^4$) were cultured under normoxic or hypoxic conditions for 26 hr. Culture supernatants were then analyzed using the Lactate Assay Kit (BioVision) following the manufacturer's instructions.

Statistical Analysis

Data are presented as means ± SD unless stated otherwise. Statistical significance was determined by Tukey's multiple comparison test. To compare two-group experiments, we used the two-tailed Student's t test.

SUPPLEMENTAL INFORMATION

Supplemental Information for this article includes seven figures and can be found with this article online at http://dx.doi.org/10.1016/j.stem.2012.10.011.

ACKNOWLEDGMENTS

We thank T. Kitamura for providing the Plat-E packaging cell line and pMY-IRES-EGFP vector, K. Rajewsky for providing *Mx1-Cre* mice, Primetech for OCR analysis by XF96, V. Haase for providing *VHL*$^{flox/flox}$ mice, R.A. Harris for providing *Pdk2*$^{-/-}$*:Pdk4*$^{-/-}$ mice, and T. Muraki, K. Igarashi, K. Saito, and T. Hirose for technical support and laboratory management. K.T. is supported by the Global COE Programs for Human Metabolomic Systems Biology (for M.S.) and for Stem Cell Medicine and in part by a MEXT Grant-in-Aid for Young Scientists (A). A.H. and M.S. were supported in part by a MEXT Grant-in-Aid for Creative Scientific Research (17GS0419). FACS analysis was supported by M.S., the Leader of the JST, ERATO, and Suematsu Gas Biology Project. T.S. and K.T. were supported in part by a MEXT Grant-in-Aid for Scientific Research (A), a MEXT Grant-in-Aid for Scientific Research on Innovative Areas, and the Project for Realization of Regenerative Medicine from MEXT.

Received: July 13, 2011
Revised: July 2, 2012
Accepted: October 12, 2012
Published: January 2, 2013

REFERENCES

Allen, C., Büttner, S., Aragon, A.D., Thomas, J.A., Meirelles, O., Jaetao, J.E., Benn, D., Ruby, S.W., Veenhuis, M., Madeo, F., and Werner-Washburne, M. (2006). Isolation of quiescent and nonquiescent cells from yeast stationary-phase cultures. J. Cell Biol. *174*, 89–100.

Arai, F., Hirao, A., Ohmura, M., Sato, H., Matsuoka, S., Takubo, K., Ito, K., Koh, G.Y., and Suda, T. (2004). Tie2/angiopoietin-1 signaling regulates hematopoietic stem cell quiescence in the bone marrow niche. Cell *118*, 149–161.

DeBerardinis, R.J., Lum, J.J., Hatzivassiliou, G., and Thompson, C.B. (2008). The biology of cancer: metabolic reprogramming fuels cell growth and proliferation. Cell Metab. *7*, 11–20.

Dunford, E.C., Herbst, E.A., Jeoung, N.H., Gittings, W., Inglis, J.G., Vandenboom, R., LeBlanc, P.J., Harris, R.A., and Peters, S.J. (2011). PDH activation during in vitro muscle contractions in PDH kinase 2 knockout mice: effect of PDH kinase 1 compensation. Am. J. Physiol. Regul. Integr. Comp. Physiol. *300*, R1487–R1493.

Fukuda, R., Zhang, H., Kim, J.W., Shimoda, L., Dang, C.V., and Semenza, G.L. (2007). HIF-1 regulates cytochrome oxidase subunits to optimize efficiency of respiration in hypoxic cells. Cell *129*, 111–122.

Gan, B., Hu, J., Jiang, S., Liu, Y., Sahin, E., Zhuang, L., Fletcher-Sananikone, E., Colla, S., Wang, Y.A., Chin, L., and Depinho, R.A. (2010). Lkb1 regulates quiescence and metabolic homeostasis of haematopoietic stem cells. Nature *468*, 701–704.

Goodell, M.A., Brose, K., Paradis, G., Conner, A.S., and Mulligan, R.C. (1996). Isolation and functional properties of murine hematopoietic stem cells that are replicating in vivo. J. Exp. Med. *183*, 1797–1806.

Goodell, M.A., Rosenzweig, M., Kim, H., Marks, D.F., DeMaria, M., Paradis, G., Grupp, S.A., Sieff, C.A., Mulligan, R.C., and Johnson, R.P. (1997). Dye efflux studies suggest that hematopoietic stem cells expressing low or undetectable levels of CD34 antigen exist in multiple species. Nat. Med. *3*, 1337–1345.

Gurumurthy, S., Xie, S.Z., Alagesan, B., Kim, J., Yusuf, R.Z., Saez, B., Tzatsos, A., Ozsolak, F., Milos, P., Ferrari, F., et al. (2010). The Lkb1 metabolic sensor maintains haematopoietic stem cell survival. Nature *468*, 659–663.

Harris, R.A., Bowker-Kinley, M.M., Huang, B., and Wu, P. (2002). Regulation of the activity of the pyruvate dehydrogenase complex. Adv. Enzyme Regul. *42*, 249–259.

Janzen, V., Forkert, R., Fleming, H.E., Saito, Y., Waring, M.T., Dombkowski, D.M., Cheng, T., DePinho, R.A., Sharpless, N.E., and Scadden, D.T. (2006). Stem-cell ageing modified by the cyclin-dependent kinase inhibitor p16INK4a. Nature *443*, 421–426.

Jeoung, N.H., Wu, P., Joshi, M.A., Jaskiewicz, J., Bock, C.B., Depaoli-Roach, A.A., and Harris, R.A. (2006). Role of pyruvate dehydrogenase kinase

isoenzyme 4 (PDHK4) in glucose homoeostasis during starvation. Biochem J *397*, 417–425.

Jones, R.G., and Thompson, C.B. (2009). Tumor suppressors and cell metabolism: a recipe for cancer growth. Genes Dev. *23*, 537–548.

Kim, M., Cooper, D.D., Hayes, S.F., and Spangrude, G.J. (1998). Rhodamine-123 staining in hematopoietic stem cells of young mice indicates mitochondrial activation rather than dye efflux. Blood *91*, 4106–4117.

Kim, J.W., Tchernyshyov, I., Semenza, G.L., and Dang, C.V. (2006). HIF-1-mediated expression of pyruvate dehydrogenase kinase: a metabolic switch required for cellular adaptation to hypoxia. Cell Metab. *3*, 177–185.

Klosinska, M.M., Crutchfield, C.A., Bradley, P.H., Rabinowitz, J.D., and Broach, J.R. (2011). Yeast cells can access distinct quiescent states. Genes Dev. *25*, 336–349.

Kobayashi, C.I., and Suda, T. (2012). Regulation of reactive oxygen species in stem cells and cancer stem cells. J. Cell. Physiol. *227*, 421–430.

Laber, B., and Amrhein, N. (1987). Metabolism of 1-aminoethylphosphinate generates acetylphosphinate, a potent inhibitor of pyruvate dehydrogenase. Biochem. J. *248*, 351–358.

Laporte, D., Lebaudy, A., Sahin, A., Pinson, B., Ceschin, J., Daignan-Fornier, B., and Sagot, I. (2011). Metabolic status rather than cell cycle signals control quiescence entry and exit. J. Cell Biol. *192*, 949–957.

Liu, J., Cao, L., Chen, J., Song, S., Lee, I.H., Quijano, C., Liu, H., Keyvanfar, K., Chen, H., Cao, L.Y., et al. (2009). Bmi1 regulates mitochondrial function and the DNA damage response pathway. Nature *459*, 387–392.

Lum, J.J., Bui, T., Gruber, M., Gordan, J.D., DeBerardinis, R.J., Covello, K.L., Simon, M.C., and Thompson, C.B. (2007). The transcription factor HIF-1alpha plays a critical role in the growth factor-dependent regulation of both aerobic and anaerobic glycolysis. Genes Dev. *21*, 1037–1049.

Miharada, K., Karlsson, G., Rehn, M., Rörby, E., Siva, K., Cammenga, J., and Karlsson, S. (2011). Cripto regulates hematopoietic stem cells as a hypoxic-niche-related factor through cell surface receptor GRP78. Cell Stem Cell *9*, 330–344.

Miyamoto, K., Araki, K.Y., Naka, K., Arai, F., Takubo, K., Yamazaki, S., Matsuoka, S., Miyamoto, T., Ito, K., Ohmura, M., et al. (2007). Foxo3a is essential for maintenance of the hematopoietic stem cell pool. Cell Stem Cell *1*, 101–112.

Nakada, D., Saunders, T.L., and Morrison, S.J. (2010). Lkb1 regulates cell cycle and energy metabolism in haematopoietic stem cells. Nature *468*, 653–658.

Nemeria, N.S., Korotchkina, L.G., Chakraborty, S., Patel, M.S., and Jordan, F. (2006). Acetylphosphinate is the most potent mechanism-based substrate-like inhibitor of both the human and Escherichia coli pyruvate dehydrogenase components of the pyruvate dehydrogenase complex. Bioorg. Chem. *34*, 362–379.

Noda, S., Horiguchi, K., Ichikawa, H., and Miyoshi, H. (2008). Repopulating activity of ex vivo-expanded murine hematopoietic stem cells resides in the CD48-c-Kit+Sca-1+lineage marker- cell population. Stem Cells *26*, 646–655.

Norddahl, G.L., Pronk, C.J., Wahlestedt, M., Sten, G., Nygren, J.M., Ugale, A., Sigvardsson, M., and Bryder, D. (2011). Accumulating mitochondrial DNA mutations drive premature hematopoietic aging phenotypes distinct from physiological stem cell aging. Cell Stem Cell *8*, 499–510.

Nosaka, T., Kawashima, T., Misawa, K., Ikuta, K., Mui, A.L., and Kitamura, T. (1999). STAT5 as a molecular regulator of proliferation, differentiation and apoptosis in hematopoietic cells. EMBO J. *18*, 4754–4765.

Papandreou, I., Cairns, R.A., Fontana, L., Lim, A.L., and Denko, N.C. (2006). HIF-1 mediates adaptation to hypoxia by actively downregulating mitochondrial oxygen consumption. Cell Metab. *3*, 187–197.

Parmar, K., Mauch, P., Vergilio, J.A., Sackstein, R., and Down, J.D. (2007). Distribution of hematopoietic stem cells in the bone marrow according to regional hypoxia. Proc. Natl. Acad. Sci. USA *104*, 5431–5436.

Sahin, E., Colla, S., Liesa, M., Moslehi, J., Müller, F.L., Guo, M., Cooper, M., Kotton, D., Fabian, A.J., Walkey, C., et al. (2011). Telomere dysfunction induces metabolic and mitochondrial compromise. Nature *470*, 359–365.

Seita, J., and Weissman, I.L. (2010). Hematopoietic stem cell: self-renewal versus differentiation. Wiley Interdiscip Rev Syst Biol Med *2*, 640–653.

Semenza, G.L. (2010). Oxygen homeostasis. Wiley Interdiscip Rev Syst Biol Med *2*, 336–361.

Shintani, T., Iwabuchi, T., Soga, T., Kato, Y., Yamamoto, T., Takano, N., Hishiki, T., Ueno, Y., Ikeda, S., Sakuragawa, T., et al. (2009). Cystathionine beta-synthase as a carbon monoxide-sensitive regulator of bile excretion. Hepatology *49*, 141–150.

Simsek, T., Kocabas, F., Zheng, J., Deberardinis, R.J., Mahmoud, A.I., Olson, E.N., Schneider, J.W., Zhang, C.C., and Sadek, H.A. (2010). The distinct metabolic profile of hematopoietic stem cells reflects their location in a hypoxic niche. Cell Stem Cell *7*, 380–390.

Soga, T., Ohashi, Y., Ueno, Y., Naraoka, H., Tomita, M., and Nishioka, T. (2003). Quantitative metabolome analysis using capillary electrophoresis mass spectrometry. J. Proteome Res. *2*, 488–494.

Soga, T., Baran, R., Suematsu, M., Ueno, Y., Ikeda, S., Sakurakawa, T., Kakazu, Y., Ishikawa, T., Robert, M., Nishioka, T., and Tomita, M. (2006). Differential metabolomics reveals ophthalmic acid as an oxidative stress biomarker indicating hepatic glutathione consumption. J. Biol. Chem. *281*, 16768–16776.

Suda, T., Takubo, K., and Semenza, G.L. (2011). Metabolic regulation of hematopoietic stem cells in the hypoxic niche. Cell Stem Cell *9*, 298–310.

Suematsu, M., Suzuki, H., Ishii, H., Kato, S., Yanagisawa, T., Asako, H., Suzuki, M., and Tsuchiya, M. (1992). Early midzonal oxidative stress preceding cell death in hypoperfused rat liver. Gastroenterology *103*, 994–1001.

Takahashi, A., Ohtani, N., Yamakoshi, K., Iida, S., Tahara, H., Nakayama, K., Nakayama, K.I., Ide, T., Saya, H., and Hara, E. (2006). Mitogenic signalling and the p16INK4a-Rb pathway cooperate to enforce irreversible cellular senescence. Nat. Cell Biol. *8*, 1291–1297.

Takubo, K., Ohmura, M., Azuma, M., Nagamatsu, G., Yamada, W., Arai, F., Hirao, A., and Suda, T. (2008). Stem cell defects in ATM-deficient undifferentiated spermatogonia through DNA damage-induced cell-cycle arrest. Cell Stem Cell *2*, 170–182.

Takubo, K., Goda, N., Yamada, W., Iriuchishima, H., Ikeda, E., Kubota, Y., Shima, H., Johnson, R.S., Hirao, A., Suematsu, M., and Suda, T. (2010). Regulation of the HIF-1alpha level is essential for hematopoietic stem cells. Cell Stem Cell *7*, 391–402.

Voet, D., and Voet, J.G. (2010). Biochemistry (Hoboken, NJ: Wiley).

Zhang, H., Gao, P., Fukuda, R., Kumar, G., Krishnamachary, B., Zeller, K.I., Dang, C.V., and Semenza, G.L. (2007). HIF-1 inhibits mitochondrial biogenesis and cellular respiration in VHL-deficient renal cell carcinoma by repression of C-MYC activity. Cancer Cell *11*, 407–420.

Zhang, H., Bosch-Marce, M., Shimoda, L.A., Tan, Y.S., Baek, J.H., Wesley, J.B., Gonzalez, F.J., and Semenza, G.L. (2008). Mitochondrial autophagy is an HIF-1-dependent adaptive metabolic response to hypoxia. J. Biol. Chem. *283*, 10892–10903.

Zhou, S., Schuetz, J.D., Bunting, K.D., Colapietro, A.M., Sampath, J., Morris, J.J., Lagutina, I., Grosveld, G.C., Osawa, M., Nakauchi, H., and Sorrentino, B.P. (2001). The ABC transporter Bcrp1/ABCG2 is expressed in a wide variety of stem cells and is a molecular determinant of the side-population phenotype. Nat. Med. *7*, 1028–1034.

Zon, L.I. (2008). Intrinsic and extrinsic control of haematopoietic stem-cell self-renewal. Nature *453*, 306–313.

Zwerschke, W., Mazurek, S., Stöckl, P., Hütter, E., Eigenbrodt, E., and Jansen-Dürr, P. (2003). Metabolic analysis of senescent human fibroblasts reveals a role for AMP in cellular senescence. Biochem. J. *376*, 403–411.